Numerical analysis of force-feedback control in a circular tank

gyongy, istvan; bruce, tom; Bryden, Ian

Published in:
Elsevier Applied Ocean Research
Publication date:
2014

Applied Ocean Research 47 (2014) 329–343

Contents lists available at ScienceDirect

Applied Ocean Research

journal homepage: www.elsevier.com/locate/apor

Numerical analysis of force-feedback control in a circular tank

Istvan Gyongy[a,*], Tom Bruce[a], Ian Bryden[b]

[a] Institute for Energy Systems, School of Engineering and Electronics, The University of Edinburgh, Edinburgh EH9 3JL, UK
[b] Research & Enterprise Office, The University of the Highlands and Islands, Ness Walk, Inverness IV3 5SQ, UK

ARTICLE INFO

Article history:
Received 20 February 2014
Received in revised form 4 July 2014
Accepted 6 July 2014
Available online 31 July 2014

Keywords:
Wave tank
Wave basin
Wave-maker theory
Force-feedback control
Wave absorption
WAMIT

ABSTRACT

The advent of circular wave tanks, with wave-making segments all around the perimeter, brings potential advantages over standard, rectangular wave tanks where the wave-maker is confined to one or two adjacent sides of the tank. It is now possible to reproduce seas with full 360° directionality, enhancing the range of possible test scenarios. However, this additional capability also presents technical challenges: waves generated on "one side" of the tank must be absorbed on the opposite side, together with any waves reflected or radiated by the model under test, to prevent contamination of the wave field. This paper reviews the theory of wave generation and absorption in a circular tank, before proceeding to identify an appropriate control scheme for the University of Edinburgh's "FloWave" combined wave/current basin. Numerical simulations, based on linear multi-chromatic waves, are carried out using WAMIT to assess the suitability of wave-maker control schemes suggested in literature. For the first time a round tank's ability to reproduce sea spectra is assessed numerically. The simulations suggest that the generation of "peaked" spectra is possible to an accurate degree, with an overall standard deviation error of less than 2% over a designated "test zone". However, there are difficulties in producing "wide" spectra, as effective dynamic wave absorption cannot be ensured over the whole frequency range. This may have important repercussions, not just for the usage of FloWave, but also in terms of the design of future round basins.

1. Introduction

There are numerous wave tank facilities in the world capable of generating multi-directional waves through the computer-controlled, serpentine motion of a segmented wave-maker along the perimeter of the tank. Typically these tanks are of rectangular shape, with wave-making panels on one or two adjacent sides of the tank, and absorbing beaches on one or more of the remaining sides. Indeed much of the theory developed for the control of segmented wave-makers assumes a rectangular tank, and/or a linear arrangement of wave-making panels. However, the requirement for a wider range of wave directions, as well as more compact tank size, has led to the development of circular tanks. In these tanks, the wave-maker extends around the entire rim, and the wave-making segments are able to generate as well as absorb waves, allowing the simulation of seas with any combination of wave directions. Examples of circular tanks described in literature include the Deep Sea Basin at the National Maritime Research Institute in Tokyo [1], the AMOEBA tank in Osaka [2], and FloWave TT [3], a combined current and wave test basin recently constructed at Edinburgh. Table 1 compares the main features of these tanks.

This paper considers wave-making in the FloWave test facility. The basin, designed for model testing at approximately 1:20 scale, comprises an array of 168 dry back, flap-type wave boards. Force-feedback control is used, which is considered to have advantages over position-control, in that the spurious harmonic content in the wave field tends to be reduced [4]. Moreover, force-feedback control lends itself better to wave absorption, which can be implemented through the simple addition of a velocity feedback loop in the control system [5]. Currents in FloWave are generated using a set of 28 impellers that pump water into and out of test area via turning vanes, the flow being recirculated through a plenum chamber, as shown in Fig. 1. The turning vane layout is designed to leave an undisturbed region directly in front of the wave boards, so as currents do not to interfere with the wave generation or absorption process.

Here it is assumed that solely waves are generated in the tank, and a thorough review is carried out of linear wave generation and absorption, as applicable to the control of a round tank. Numerical computations are then carried out to assess a number of possible control schemes for the tank, in terms of the resulting steady state behaviour.

In its typical operating scenario, FloWave is expected to reproduce realistic sea spectra. Ideally, the generated sea should extend

* Corresponding author. Tel.: +44 1316508689.
E-mail addresses: istvan.gyongy@ed.ac.uk, istvan.gyongy@gmail.com (I. Gyongy), tom.bruce@ed.ac.uk (T. Bruce), ian.bryden@uhi.ac.uk (I. Bryden).

0141-1187/$ – see front matter © 2014 Elsevier Ltd. All rights reserved.
http://dx.doi.org/10.1016/j.apor.2014.07.002

Table 1
Characteristics of circular tanks.

Tank	FloWave TT [3]	NMRI [1]	AMOEBA [2]
Diameter	25 m	14 m	1.6 m
Actuator	168 force-feedback, dry back paddles	128 position-feedback, wet back paddles	50 force-feedback plungers
Depth	2 m	5 m	0.25 m
Maximum wave height	0.7 m (planned)	0.5 m	0.02 m
Wave period range	1–3 s (planned)	0.5–4 s	0.33–0.625 s

over a large proportion of the tank, allowing for the testing of large scale models or device arrays. The present paper makes the following important contributions in assessing the prospective capabilities of the tank:

- The ability of the tank to reproduce sea spectra in a spatially uniform manner is investigated.
- The impact of a single malfunctioning paddle on the generated sea spectra is explored.
- The response of a floating body in the middle of the tank is considered, and compared with the expected body motion given the prescribed sea spectrum.

The present paper contains the first numerical study of a round tank generating multi-chromatic waves, and whilst the focus is on FloWave, the results and methodology are relevant for round tanks in general.

To simulate the tank, the approach of Newman [6], based on the commercial boundary element method (BEM) solver WAMIT, is applied. The approach has been validated experimentally for a 96° arc of paddles in the Edinburgh Curved Tank by Gyongy et al. [7]. A key advantage of using a linear diffraction solver, is that it is simple to apply to a circular (or indeed any) tank geometry. Moreover, it lends itself well to modelling force-control, as the hydrodynamic forces on the paddles, and the associated paddle motions, are easily established. Given the linearity of the approach, the waves from each paddle may be computed separately, and then superposition applied to obtain the overall wave field.

Other methods for analysing linear wave-making in a tank include analytical approaches modelling the individual paddles as point sources or finite width sources [8,9], or the collection of paddle faces as one continuous surface. Whilst most techniques assume position-controlled wave-makers (with given motions imposed), Spinneken et al. [4] consider the force-control of a rectangular tank with absorbing wave-makers, deriving a theoretical first-order transfer function backed up by experimental observations. A drawback of analytical approaches is that reflections can be difficult to model. In a simpler scenario, when the line of wave-makers faces a bank of absorbing beaches (as in a typical rectangular tank), the reflecting side walls may be readily accounted for [10]. However, analysing reflections (and re-reflections) off a round boundary, or indeed the effect of an object in the tank on the wave field, would be too complex. An alternative, numerical option is to use a spectral method [11].

It is important to note that the linear waves analysed here only represent a subset of the test scenarios that a wave basin is expected to provide. Indeed, one of the rationales behind physical testing is that it allows non-linear wave/structure interactions to be examined, which are often difficult to analyse numerically in a reliable way. Hence there is a requirement to reproduce non-linear, in particular high steepness waves, in an accurate wave. This paper, in staying in the domain of linear waves, is intended to constitute a first step in identifying a viable control scheme for FloWave, and a discussion is included on the implications of generating non-linear waves.

The paper is organised as follows. Section 2 reviews the theory for controlling a circular wave tank, with absorbing, force-feedback paddles. A basic physical model for wave boards is first outlined, followed by the control loop around wave boards. Potential control strategies for the whole tank are then discussed. In Section 3, the methodology of simulating force-control and dynamic absorption in a circular tank using WAMIT is described. Section 4 presents the results of simulations, both for the control of the "empty" FloWave basin and for the case of a floating object in the tank, which results in radiated and diffracted waves. Section 5 discusses non-linear waves. Conclusions are given in Section 6.

2. Modelling a circular tank

2.1. Paddle dynamics

As outlined in Spinneken et al. [12], a flap-type wave board, depicted in Fig. 2, may be considered as an inverted pendulum with mass m and inertia r. The tangential weight component is

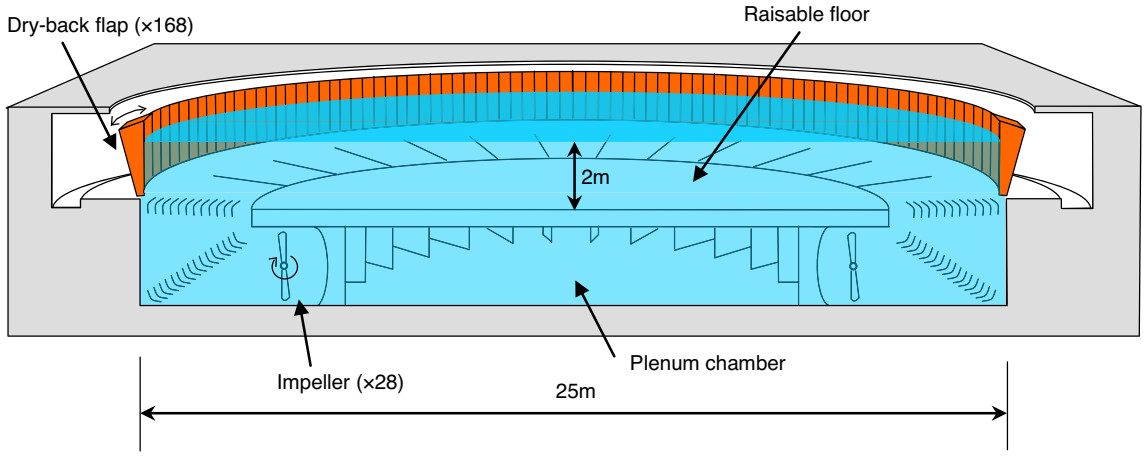

Fig. 1. Cross-sectional diagram of FloWave TT.

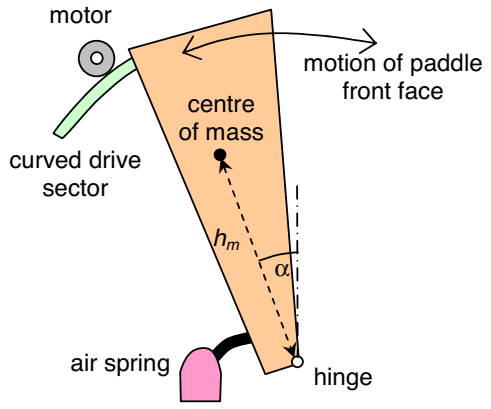

Fig. 2. A flap-type wave-making paddle.

$mgh_m \sin\alpha$, where h_m is the distance from the hinge to the centre of mass, and α is the inclination of the line joining the centre mass and the hinge, with respect to the vertical. For small paddle rotations the approximation $\sin\alpha \approx \alpha$ may be used. When the paddle is in motion, radiating waves, it experiences a hydrodynamic added inertia r_Φ and added damping d_Φ, and incident waves apply a certain exciting torque T_w about the hinge axis. The paddle is also subject to an external control torque T_c (provided by the drive motor) and the paddle mechanism has a certain rotational stiffness c (the mechanical damping is assumed to be negligible compared with the hydrodynamic damping). In the case of FloWave, the stiffness comes mainly from "air springs" connected to the paddles, whose function is to balance the hydrostatic loading (and tangential weight component of the paddle) such that the rest position of the paddle face is vertical.

Based on the above, the motion of the paddle may be expressed in terms of the paddle angle $\theta(t)$ as

$$(r + r_\Phi)\ddot{\theta} + d_\Phi\dot{\theta} + (c - mgh_m)\theta = T_w + T_c. \tag{1}$$

In the equation above it is assumed that the hydrostatic loading is constant (and independent upon θ), which is correct to a first order approximation. Fig. 3 shows a schematic diagram of the paddle, indicating the paddle angle $\theta(t)$, and the hinge depth H and water depth h. Note that the horizontal displacement X_o of the paddle face at the static water level can be related to θ as

$$X_o = H\ \tan\theta \approx H\theta, \tag{2}$$

where a small angle approximation has been used. If the paddle is oscillating sinusoidally with angular frequency ω and amplitude

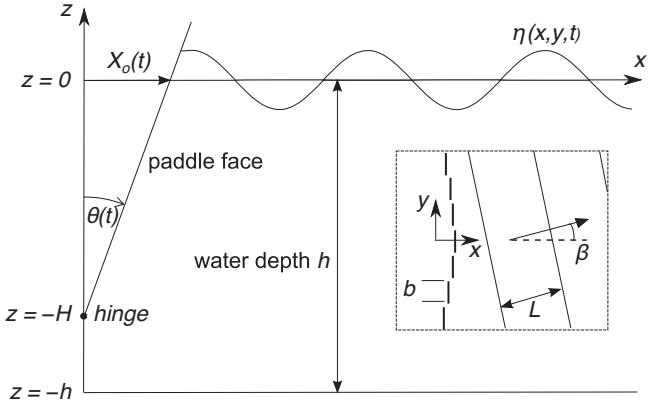

Fig. 3. Schematic side view of a paddle and overhead view (inset) of a linear array of paddles generating a plane wave.

X_a at the still water level, then the horizontal displacement may be expressed in terms of vertical position as

$$X = \frac{X_a}{2} f(z) e^{i\omega t} + c.c., \tag{3}$$

where *c.c.* refers to the complex conjugate of the preceding term, and

$$f(z) = \begin{cases} \dfrac{z+H}{H} & \text{for } 0 \geq z \geq -H, \\ 0 & \text{for } z < -H. \end{cases} \tag{4}$$

For theoretical analyses, the hydrodynamic coefficients r_Φ, d_Φ in Eq. (1) are typically evaluated by assuming that the wave board forms part of an infinitely long, segmented wave-maker (facing a fluid domain that extends to infinity), which is generating regular, oblique waves. In contrast to the circular FloWave tank, in most analyses the wave-making segments are assumed to be arranged in a straight line. Furthermore, the width b of individual segments is taken to be negligible as compared to the wavelength L of the generated wave, so that the velocity distribution along the wave-maker may be represented by a continuous function.

Subject to the above assumptions, together with the assumptions of linear wave-maker theory, the hydrodynamic coefficients for a wave frequency ω and direction β are given by (see, for example, Newman [6])

$$r_\Phi = 4b\rho \sum_{n=1}^{\infty} \frac{c_n^2 (k_n / \sqrt{k_n^2 + k_o^2 \sin^2\ \beta})}{\sin\ 2k_n h + 2k_n h}, \tag{5}$$

$$d_\Phi = 4b\rho\omega \frac{c_o^2\ \sec\ \beta}{\sinh\ 2k_o h + 2k_o h}, \tag{6}$$

where ρ is the density of the fluid, k_o is the positive real root and k_n are the positive imaginary roots of the dispersion equation

$$\omega^2 = gk\ \tanh\ kh, \tag{7}$$

and the parameters c_o and c_n are given by

$$\begin{aligned} c_o &= \int_{-h}^{0} Hf(z)\ \cosh\ k_o(z+h)\ dz \\ &= \frac{k_o H\ \sinh\ k_o h - \cosh\ k_o h + \cosh\ k_o(h-H)}{k_o^2}, \end{aligned} \tag{8}$$

$$\begin{aligned} c_n &= \int_{-h}^{0} Hf(z)\ \cos\ k_n(z+h)\ dz \\ &= \frac{k_n H\ \sin\ k_n h + \cos\ k_n h - \cos\ k_n(h-H)}{k_n^2}. \end{aligned} \tag{9}$$

Note that r_Φ, d_Φ contain an additional factor of H^2 compared with the added mass and damping coefficients given in Newman [6], as the latter are defined with respect to the linear dynamics of the paddle at the still water level, rather the rotational dynamics as given by Eq. (1). Note also that the results in Newman [6] are per unit paddle width. The added inertia r_Φ results from the evanescent, standing waves that are generated by the paddle (and the associated body of water that is accelerated), whilst the added damping d_Φ is due to the radiated progressive wave, and is related to the energy transferred away.

The wave angle β is specified relative to the x-axis as shown in the inset of Fig. 3, so that $\beta = 0°$ refers to a wave propagating normally to the wave board. In the case when waves are generated with $\beta = 0°$ (so that all wave-maker segments move identically, a scenario analogous to a 2D flume) the predicted far-field wave amplitude is

$$A_f = \frac{4k_o c_o X_a}{H} \left[\frac{\sinh\ k_o h}{\sinh\ 2k_o h + 2k_o h}\right], \tag{10}$$

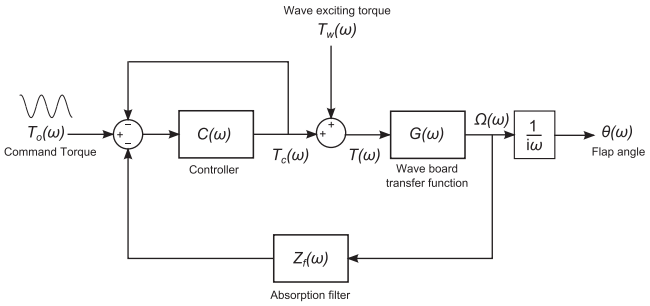

Fig. 4. Block diagram of paddle control system.

where X_a is the amplitude of the paddle displacement at the still water level.

2.2. Control of individual paddles

The control of absorbing, force-feedback wave boards is discussed in detail by Spinneken et al. [12] and Naito [13], in the context of a 2D flume and 3D basin, respectively. Here it is again assumed that the wave board is part of a segmented, wave-maker, and there is now an incident wave of angle β (as depicted in the inset of Fig. 3 but travelling in the opposite direction).

For a flap-type wave board, the control system may be represented by the block diagram in Fig. 4. The constituent parts of this system, considered in the frequency domain, are the controller $C(\omega)$ (which is taken here to include the dynamics of the motor driving the paddle), the wave board transfer function $G(\omega)$, and the absorption filter $Z_f(\omega)$ that provides absorption of incident waves. All of these elements are taken to be linear.

The input to the system is a command torque T_o, from which velocity and torque feedback signals are subtracted (the former being passed through $Z_f(\omega)$ first). The resulting signal is fed to the controller $C(\omega)$, which in turn applies a torque T_c on the paddle (as measured by a load cell or similar). Waves arriving at the paddle exert an additional torque T_w, so that the total "external torque" acting on the paddle assembly is $T(\omega) = T_c + T_w$. The relationship between this torque and the resulting paddle velocity $\Omega(\omega)$ (typically measured using a tachogenerator) is represented by $G(\omega)$ in the block diagram. The output of the system is the flap angle $\theta = \Omega(\omega)/i\omega$.

From Eq. (1), the transfer function $G(\omega)$ is given by

$$G(\omega) = \frac{\Omega(\omega)}{T(\omega)} = \frac{1}{(r + r_\Phi)i\omega + d_\Phi + c'/i\omega}, \tag{11}$$

where $c' = (c - mgh_m)$ is the effective stiffness of the paddle mechanism.

The inner loop, involving the controller $C(\omega)$, has an effective transfer function of $C(\omega)/(1 + C(\omega))$. An ideal controller must ensure that the torque T_c applied on the paddle, follows closely that prescribed by the T_o, minus the absorption filter signal or "absorption torque". This requires $C(\omega)$ to be very large, making $C(\omega)/(1 + C(\omega))$ close to unity. Thus, assuming an ideal controller, the inner loop may be approximated by a simple forward path with unity gain [14]. In this case the transfer function $F(\omega)$ of the entire system, from the command torque $T_o(\omega)$ to the paddle angle $\theta(\omega)$ can be written as

$$F(\omega) = \frac{\theta(\omega)}{T_o(\omega)} = \frac{1}{i\omega}\frac{G(\omega)}{(1 + G(\omega)Z_f(\omega))} = \frac{1}{i\omega}\frac{1}{(Z_d(\omega) + Z_f(\omega))}, \tag{12}$$

where $Z_d(\omega) = 1/G(\omega)$ and is referred to by Spinneken et al. [12] as the "dynamic impedance" of the wave paddle. This incorporates the dynamics of the wave paddle itself, together with the wave-induced terms.

The same transfer function $F(\omega)$ applies to the path from the wave exciting torque T_w to the paddle angle $\theta(\omega)$ so that in general the paddle angle can be expressed as

$$\begin{aligned}\theta(\omega) &= F(\omega)(T_o(\omega) + T_w(\omega)) \Leftrightarrow i\omega\theta(\omega)(Z_d(\omega) + Z_f(\omega)) \\ &= T_o(\omega) + T_w(\omega).\end{aligned} \tag{13}$$

In a way akin to impedance matching in electric signal transmission, the power absorbed from incident waves is maximised when the absorption filter $Z_f(\omega)$ is the complex conjugate of $Z_d(\omega)$ [15]

$$Z_f = Z_d^*, \tag{14}$$

which, in theory, leads to full absorption. In the general case, taking the real R and imaginary Y parts of Z_f and Z_d, one can express the power absorption coefficient, defined as the absorbed power over the maximum power, as

$$\gamma = \frac{R_f R_d}{(R_f + R_d)^2 + (X_f + X_d)^2}. \tag{15}$$

The absorption filter is typically designed such that mimics a mass-spring-damper system, in which case it is of the form

$$Z_f = m_f i\omega + d_f + c_f/i\omega, \tag{16}$$

where m_f, d_f and c_f are the effective values of inertia, damping and stiffness. Thus, in physical terms, the condition given by Eq. (14) requires a filter design (or "absorption mechanism") where the external inertia and spring force afforded by the mechanism cancels the inertia and stiffness of the paddle, whilst the external damping is equal to the hydrodynamic damping:

$$m_f\omega - c_f/\omega = -(r + r_\Phi)\omega + \frac{c'}{\omega}, \tag{17}$$

$$d_f = d_\Phi. \tag{18}$$

In practice, the "spring" term is sometimes left out from the absorption filter ($c_f = 0$). Indeed analytical calculations in Maguire [16] suggest that the term makes virtually no difference as regards the absorption characteristics of a typical 2D flap-type wave-maker, apart from at very low frequencies, where Spinneken et al. [17] note that good absorption can still be important in preventing seiche waves.

As the hydrodynamic coefficients r_Φ, d_Φ in Eqs. (5) and (6) depend on the frequency (as well as the angle) of the incident waves, the filter coefficients can only be adjusted to provide an exact match (and, theoretically, full absorption) at one chosen wave frequency and direction. At all other frequencies, a proportion of the incident wave will be reflected.

Spinneken et al. [12] propose finding a "best fit" filter (in a least-square sense) over the frequency range of interest, as an alternative approach to optimising absorption at one given frequency. In numerical simulations and physical experiments in a 2D flume, the proposed method is shown to give superior absorption performance to alternative methods for setting the filter coefficients [17].

There have also been attempts to improve the effective "bandwidth" by using variable coefficients in the filter. Taking this approach, a time domain filter, optimised for irregular waves, may be derived, but causality problems arise in its practical implementation and Naito [13] argues that no significant advantage is offered over a constant coefficient filter. Chatry et al. [18] present a method where the coefficients are automatically adjusted by tracking the frequency of incident waves via a Kalman filter. The method is tested in numerical simulations, and shown to adapt successfully to the frequency of the incoming waves.

2.3. Control of wavefield in tank

The previous section introduced the main concepts around the force-control of individual wave boards in a segmented wave-maker, under the assumption that plane, oblique waves are generated by the wave-maker, and/or are incident on the wave boards. In practice, this control system is implemented on an electronic control board allocated to each wave board, with every paddle receiving a separate torque command, synthesised by a central computer that orchestrates wave fields in the tank. In FloWave TT, the absorption mechanism of the control boards may also be set individually through this computer via selection of filter coefficients.

Assuming absorption is suitably configured, to achieve control of the wave field in the tank, one must determine how sinusoidal demand signals sent to paddles should be adjusted in phase and amplitude to generate uniform waves with pre-set periods, directions and amplitudes. Once this has been established then, in principle, any given wave spectrum can be generated in the tank through linear superposition of regular waves, allowing the physical simulation of irregular, multi-directional seas.

For a general wave-maker, the paddle amplitudes and phases to obtain a regular wave with a given period and direction are usually set using simple rules derived from wave-maker theory. On the other hand, the gain – or multiplying factor – applied to the paddle signals to get the desired wave amplitude is usually based on an experimentally determined *tank transfer function*. This transfer function links the wave-board force (or amplitude, for position-controlled paddles) to the amplitude of the progressive wave. It typically exists in the form of a user-adjustable look-up table on the wave-maker computer, covering a range of wave periods and directions.

Whilst it is common to control wave-makers based on empirical transfer functions, theoretical transfer functions have been derived – and in some cases validated – for different tank configurations. Notably, Spinneken et al. [4] derive the first-order transfer function for rectangular tank with force-feedback, absorbing paddles on one side (assuming the wave-maker extends to infinity). In laboratory tests involving the generation of directional JONSWAP spectra, the use of the theoretical transfer function leads to an accurate reproduction of the target spectrum, especially at frequencies near the peak, where the maximum error in amplitude content is only around 1–2%. At higher frequencies, a deviation from the target spectrum is seen as the propagation angle is increased, which may be countered by incorporating the effects of finite wave-maker segmentation in the model. The generated spectrum is also shown to be similar to that obtained using an empirically determined transfer function, indicating that the theoretical function may replace the need for calibration in generating accurate sea states. It is however noted by Spinneken et al. [4] that there are inherent differences in the two approaches, as empirical calibration typically considers the overall wave spectrum at a certain point in a tank, including beach reflections, whereas a theoretical model generally refers to incident waves only.

Similar theoretical transfer functions and overall control strategies will now be considered for a circular tank of the type of FloWave. Crucially, in this case there are wave-making segments all around the perimeter, and thanks to the axisymmetry of the tank, it is sufficient to consider the generation of waves in one particular direction.

As in the previous sections, the paddles are flap-type with hinge depth H. There are a total of N paddles around the rim of the tank, which is of radius R. The water depth h is constant. In the first instance, it is assumed that there is no absorption mechanism in the paddles, and that the velocity distribution along the rim can be considered to be continuous (i.e. wave-maker segmentation effects

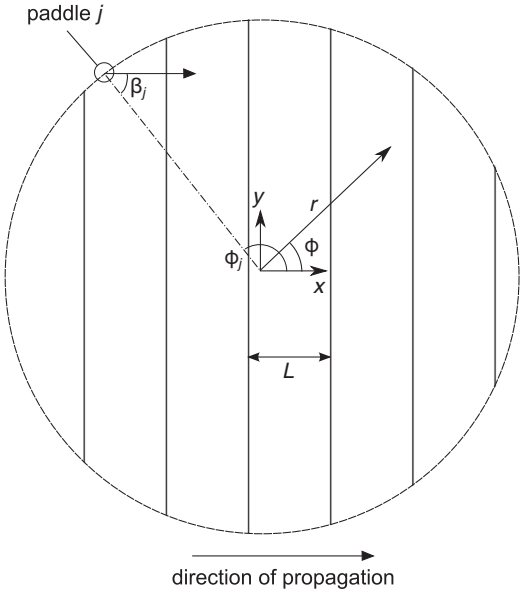

Fig. 5. Top view of tank showing the crests of a plane wave travelling in the direction of the x-axis.

can be neglected). This requires the paddle width b to be much smaller than the wavelength L of the generated waves. The effect of the gaps between neighbouring paddles (sealed using a rolling gusset) is ignored.

The coordinate system shown in Fig. 5 is adopted, featuring both polar (r,φ) and Cartesian (x,y,z) coordinates, with the origin being at the centre of the still free surface. The z-axis is directed out of the page such that $z=0$ at the still water surface, and $z=-h$ at the bottom. Under the assumptions of incompressible, inviscid and irrotational flow, potential flow theory is applied with appropriate boundary conditions. The first-order velocity potential is denoted by Φ_1, so that the first-order fluid velocity $\mathbf{u}_1$ can be expressed as $\mathbf{u}_1(r,\varphi,z,t)=\nabla\Phi_1$.

The objective is to generate progressive, plane waves in the tank. For a plane wave of frequency ω and amplitude A_f, travelling in the direction of the x-axis (as indicated in Fig. 5), the free surface elevation η may be expressed as:

$$\eta_1=\frac{A_f}{2}e^{i(\omega t-k_o x)}+c.c., \tag{19}$$

and the corresponding potential is

$$\Phi_1=\frac{igA_f}{2\omega}\frac{\cosh\,k_o(z+h)}{\cosh\,k_o h}e^{i(\omega t-k_o x)}+c.c. \tag{20}$$

The parameter k_o in the above equation is the positive real root of the dispersion relation (7).

A sensible approach for generating the above wave would be to oscillate the paddles such that the velocity variation around the rim "conforms" to the velocity field prescribed by Eq. (20). This would mean that the wave-maker velocity around the rim, and hence the displacement X_o at the still water level would have to vary as:

$$\frac{\partial X_o}{\partial t}, X_o\propto\left.\frac{\partial\Phi_1}{\partial r}\right|_{r=R}, \tag{21}$$

$$X_o(\varphi)\propto\cos\,\varphi e^{i(\omega t-k_o R\cos\varphi)}+c.c., \tag{22}$$

where the equation $x=R\cos\varphi$, referring to the geometry of the rim at rest, has been used.

Mei et al. [19] give a formal derivation of Eq. (22), for a piston-type wave-maker that extends to the bottom of the tank, using an eigenfunction expansion of the general solution for the potential

in the tank. Following their approach, but taking the wave boards to be flap-type, with a motion described by Eq. (3), the required displacement amplitude X_a at the still water level is

$$X_a = -iX_{a,2}\cos\varphi e^{-ik_oR\cos\varphi}, \tag{23}$$

where $X_{a,2}$ is the displacement amplitude of a 2D flap (see Eq. (10)) giving the specified progressive wave amplitude of A_f:

$$X_{a\cdot 2} = \frac{A_f H}{4k_o c_o}\left[\frac{\sinh 2k_oh + 2k_oh}{\sinh k_oh}\right]. \tag{24}$$

Note that X_a is now a complex quantity, incorporating the phase as well as the magnitude of the paddle displacement around the rim, both of which are modulated by $\cos\varphi$. The displacement is greatest where the rim is normal to the direction of the desired wave (at $\varphi = 0, \pi$; the magnitude there corresponding to the 2D case) and is zero where the rim is parallel to the wave (at $\varphi = \pi/2$, $3\pi/2$).

Mei et al. [19] proceed to deduce the resulting (first-order) hydrodynamic forces on a piston wave-maker, as a function of φ, subject to the approximation

$$\frac{I_m(k_nR)}{I'_m(k_nR)} \approx 1, \tag{25}$$

where k_n are the positive imaginary roots of Eq. (7), I_m is the m-th order modified Bessel function, and I'_m is the first derivative of I_m. Performing the same analysis for a flap-type wave-maker, one gets the following expression for the wave-induced torque, per unit length of the rim

$$T_h = -\frac{1}{2}\rho g A_f H^2 \frac{c_o}{H^2\cosh k_oh}(1 - iD\cos\varphi)e^{i(\omega t - k_oR\cos\varphi)} + c.c., \tag{26}$$

where

$$D = \sum_{n=1}^{\infty}\frac{c_n^2}{c_o^2}\frac{\sinh 2k_oh + 2k_oh}{\sin 2k_nh + 2k_nh}, \tag{27}$$

and c_o and c_n are given by Eqs. (8) and (9). A given paddle j will now be considered, which occupies a width b along the rim, and whose centre is positioned at an angle φ_j as indicated in Fig. 5. One may express the torque on this paddle in terms of the effective hydrodynamic added inertia $r_{\Phi,j}$ and added damping $d_{\Phi,j}$ as

$$\begin{aligned} T_hb &= -r_{\Phi,j}\ddot{\theta} - d_{\Phi,j}\dot{\theta} = \frac{1}{H}(\omega^2 r_{\Phi,j} - i\omega d_{\Phi,j})X_o \\ &= \frac{1}{2H}(\omega^2 r_{\Phi,j} - i\omega d_{\Phi,j})(X_a e^{i\omega t} + c.c.). \end{aligned} \tag{28}$$

By combining Eqs. (23), (26) and (28), one may determine expressions for $r_{\Phi,j}$, $d_{\Phi,j}$.

$$r_{\Phi,j} = 4b\rho\sum_{n=1}^{\infty}\frac{{c_n}^2}{\sin 2k_nh + 2k_nh}, \tag{29}$$

$$d_{\Phi,j} = -4b\rho\omega\frac{c_o^2\sec\varphi_j}{\sinh 2k_oh + 2k_oh}. \tag{30}$$

Thus, according to the theory of Mei et al. [13], the added inertia is constant around the rim of the tank and corresponds to the added inertia in the case of a 2D paddle (Eq. (5) with $\beta = 0$). The added damping varies with $\sec\varphi$ and for any given paddle j its value is the same as if the paddle was part of a linear array generating an oblique wave of angle $\beta_j = \varphi_j - \pi$ (see Eq. (6)), where β_j is the wave direction in the tank relative to the paddle in question (as indicated in Fig. 5).

In the hypothetical case when the dynamics of the paddle are dominated by the wave-induced inertia and damping (such that, in comparison, the paddle's mass and stiffness are negligible), the torque given by Eq. (28) represents the torque that must be applied on each of the paddles to obtain the desired propagating wave. More generally, the torque to be applied on the paddles may be expressed in the frequency domain as:

$$T_j(\omega) = Z_{d,j}(\omega)i\omega\theta_j(\omega), \tag{31}$$

where $Z_{d,j}(\omega) = (r + r_{\Phi,j})i\omega + d_{\Phi,j} + c'/(i\omega)$ is the dynamic impedance of paddle j as defined in Section 2.2 (but with the hydrodynamic coefficients given by Eqs. (29) and (30) for a round tank), and $\theta_j(\omega)$ is the prescribed paddle rotation for paddle j, as obtained from Eqs. (23) and (24), for a wave amplitude spectrum of $A(\omega)$ in the middle of the tank

$$\theta_j(\omega) = -i\frac{A(\omega)}{4k_oc_o}\left[\frac{\sinh 2k_oh + 2k_oh}{\sinh k_oh}\right]\cos\varphi_j e^{-ik_oR\cos\varphi_j}, \tag{32}$$

(where k_o varies with ω). The paddle angle φ_j in the above equation may be written as:

$$\varphi_j = \left(j - \frac{1}{2}\right)\frac{2\pi R}{N}, \quad j = 1, \ldots, N, \tag{33}$$

where N is the total number of paddles in the tank.

It is worth noting that the motion of the paddles will invariably excite additional modes to the desired travelling waves specified by Eqs. (19) and (20). There will be evanescent spurious modes, confined to the vicinity (within two/three water depths) of the paddles. Furthermore, second and higher modes will be generated (which are not considered in this paper). However, in normal tank operation, first-order progressive waves should dominate the wave field in the tank.

Fig. 6 shows a polar plot of the torque to be applied on the paddles, against paddle angle φ_j, when a wave with $k_oh = 2$ is to be generated in the tank. This equates to approximately a 2 s wave in FloWave, which is in the middle of the operating range. Three separate lines are given, corresponding to

(a) Circular tank theory (dotted line), as represented by Eq. (31),
(b) Oblique wave theory (dashed line), also denoted by Eq. (31) but with the hydrodynamic coefficents in Eqs. (5) and (6) (with $\beta = \varphi - \pi$),
(c) WAMIT tank model (full line) outlined in Section 3, which incorporates the geometry of the tank and wave-maker segmentation, and is therefore likely to be more accurate than analytical theories (a) and (b).

In all three cases, the paddles are assumed to move as per Eq. (23) and their physical properties (mass, stiffness) are neglected. The desired uniform wave travels in the direction indicated in Fig. 6, with the "upstream" (or weather) half of the rim imparting energy to, and the "downstream" (or lee) half of the rim absorbing energy from the wave system. Paddles at the interface of the two halves (whose face is close to parallel to the wave direction), must effectively be "restrained" by the wave-maker controls, otherwise excitation by the pressure variation of passing waves leads to contamination of the wave field.

It is noted from the graph that the corresponding torque plots for circular tank and oblique wave theories are essentially coincident (with a max. deviation of less than 0.1% between the two), and are similar to the results of numerical computations using WAMIT. The magnitude of the torque is seen to be largely uniform around the tank, though the torque calculated numerically drops to around 2% below the theoretical values for the paddles to the sides of the propagating waves. This deviation is likely due to wave-maker curvature and segmentation effects unaccounted for in the analytical equations.

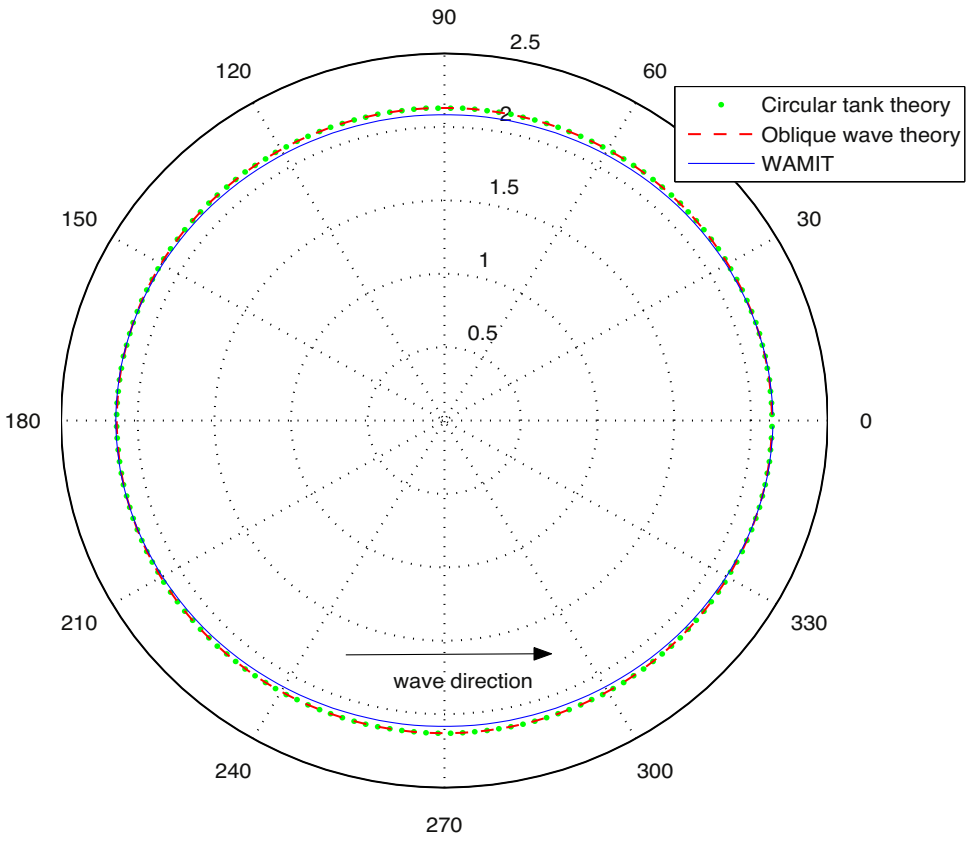

Fig. 6. Polar plot of normalised torque $|T_j|/b\rho g A_f H^2$ on paddles against paddle angle φ_j for a uniform wave with $k_o h = 2$, as predicted by circular wave theory (dotted line), oblique wave theory (dashed) and WAMIT (full line).

At first, it may seem surprising that the wave-induced torques, or equivalently in this case, the torques required to sustain the desired wave, are near-constant in magnitude around the rim (despite the paddle amplitudes varying as $\cos\varphi$). However, provided that the wave field induced by the paddle motion specified in Eq. (20) is dominated by the desired uniform, progressive wave (with negligible near-paddle, evanescent content), then all paddles will experience largely the same hydrodynamic pressures (in magnitude terms), and thus the same resultant torques.

As the wave frequency is raised, a different picture starts to emerge. The wave motion in the desired progressive wave becomes more confined to near the surface and no longer reaches as deep as the paddle motion. As a result, an increasing proportion of the torque applied on the wave-generating and absorbing paddles goes towards exciting evanescent modes, which is manifested in the predicted torque plots becoming elliptical. Wave-maker segmentation and curvature effects also become more significant at higher frequencies, leading to a departure between numerical and theoretical results. Fig. 7 illustrates these phenomena for wave with $k_o h = 6$ (approximately a 1.15 s wave in FloWave).

2.4. Practical considerations

The above control strategy, in which the wave-maker segments are oscillated "blindly" with set torques (as determined by the parameters of the desired planar wave(s)), may seem appealing due to its simplicity, but is unfortunately fraught with practical problems. Most crucially, the method does not deal with the scattered (and radiated) waves that arise when there is a model in the tank. Any such waves, when reaching the paddles, would just be reflected back, leading to standing waves and contamination of the wave field in the tank. In addition, the theory behind the control scheme in effect assumes that the phase difference between waves at the "upstream" and "downstream" sides of the tank (i.e. between the generating and absorbing sides) is known in advance, which for combined wave/current tanks (like FloWave) would not be the case.

Newman [6] uses WAMIT to assess alternative strategies for controlling a circular wave tank, which may be summarised as follows:

A. Oscillate the generating paddles (on one half of the tank) according to the pre-defined motion in Eq. (23), and program the absorbing paddles on the other half to respond to the sensed pressure variations as a "mass-damper"-type mechanism, with coefficients based on 2D wave theory (see Eqs. (16)–(18), where $c_f = 0$ in this case, and r_Φ, d_Φ are given by Eqs. (5) and (6) with $\beta = 0$).
B. As A, but with the "absorption mechanism" of each of the absorbing paddles set individually in accordance with the anticipated angle of incidence relative to the paddle. In other words, "oblique wave theory" is assumed in the configuration of the absorbers (the hydrodynamic coefficents of the paddles are again taken to be those given by Eqs. (5) and (6), but with $\beta = \varphi - \pi$, where φ is the paddle angle).
C. Oscillate all paddles as prescribed by Eq. (23) and impose additional ("correcting") motion via an absorption mechanism (based on 2D theory) that reacts to the difference between the sensed hydrodynamic torques on the paddles, and the expected values of these torques (corresponding to the paddle motions of Eq. (23) in the "baseline" tank). The aim is to absorb any

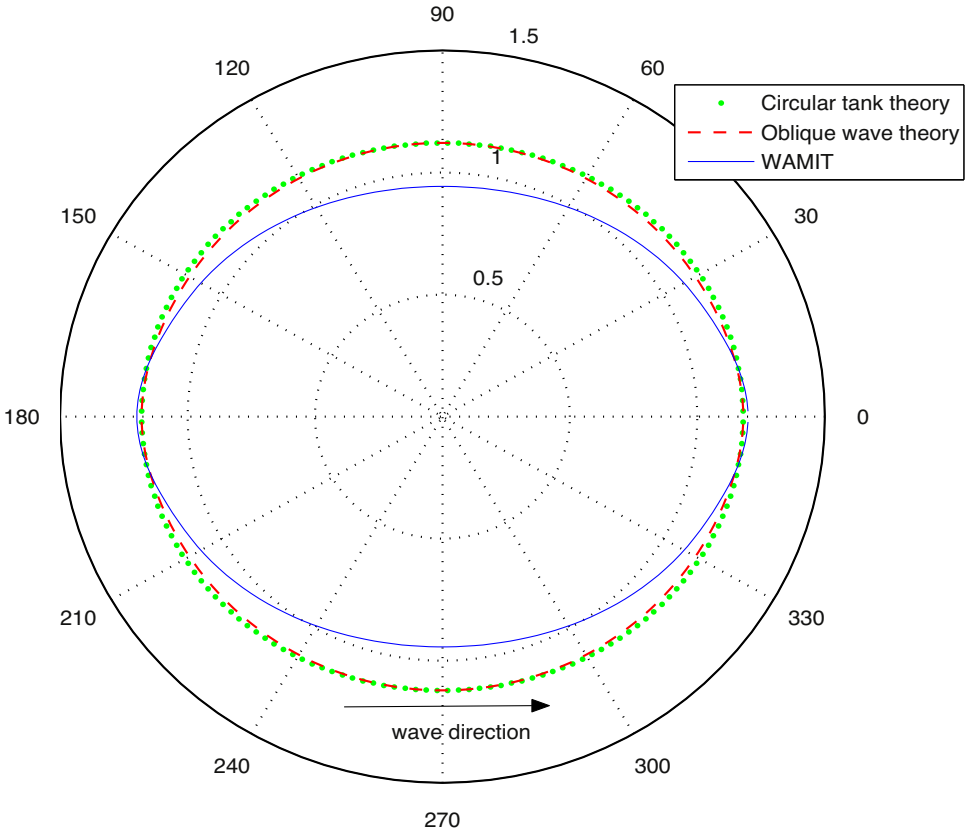

Fig. 7. Polar plot of normalised torque $|T_j|/\mathrm{b}\rho g A_f H^2$ on paddles against paddle angle φ_j for a uniform wave with $k_o h = 6$, as predicted by circular wave theory (dotted line), oblique wave theory (dashed) and WAMIT (full line).

waves arising from disturbances of the generated wave system, for example, due to a model in the tank.

In frequency domain simulations involving the generation of monochromatic, unidirectional waves, method B is shown to produce a uniform, progressive wave field, whereas method A leads to significant standing wave content in the tank. In the case when a floating hemisphere is present in the tank, method C successfully absorbs radiated and scattered waves.

To the authors' knowledge, the approaches have yet to be tested in experiments and whilst they are more realistic than the original control scheme, practical issues still remain in their implementation. Splitting the paddles in half into position-controlled and force(/velocity) controlled segments (as in methods A and B) or conferring varying absorption parameters to the paddles according to their position (method B), is not viable if multi-directional wave fronts are to be generated. Furthermore, it not known how method C would perform in practice in the case of significant disturbances in the tank (such as strong currents generated in FloWave), when the true hydrodynamic torques on the paddles may deviate considerably from the expected values. In such a case the practice of prescribing wave-generating signals to all paddles, including to those on the downstream side, when trying to produce a unidirectional wave, may in fact lead to an increase in unwanted waves. It is also worth pointing out that all the simulations in Newman [5] are for one frequency at a time, to which the absorption mechanism is tuned, and there is no indication of how the control schemes would perform for multi-chromatic waves.

A simple control scheme that has been tested in practice is the method used in the compact AMOEBA tank [13], where each plunger is tuned indentically and can partake in both the generation and absorption of waves simultanously. Minoura et al. [2] present a first-order theory for generating arbirary wave fields in a tank of this kind. Each wave-making element is taken to produce a ring wave, whose contribution to the overall wavefield is expressed using Hankel functions. Evanescent waves are neglected and perfect wave absorption is assumed. In experiments in which circular and elliptic configurations of the AMOEBA were used to generate regular, long-crested waves, the theory was found to give reasonably good wave height predictions for points further than a wavelength away from the wave-maker. Results given for a 2 Hz wave indicate a maximum wave height error of around 10–20% at said points. Previous studies on the wave exciting forces experienced by models in the tank when generating irregular waves also yielded positive results [20].

According to the theory of Minoura et al. [2], to compose a planar wave travelling in the direction of the x-axis (as specified by Eq. (19)), the (wave-generating) command torques $T_{o,j}$ sent to the N wave-making segments should be:

$$T_{o,j}(t) = \frac{1}{2}\sum_{n=-\infty}^{\infty} I(\omega)\frac{i^n e^{in\varphi_j}}{H_n^{(1)}(k_o R)}\frac{b}{2\pi R}e^{i\omega t} + c.c., \quad j = 1, \ldots, N, \qquad (34)$$

where $I(\omega)$ is a transfer function relating the torque applied to a paddle to the ensuing wave amplitudes, and $H_n^{(1)}$ is the n-th order Hankel function. The magnitude of $T_{o,j}$ has a "raised cosine-like" profile around the circumference of the tank, as depicted in Minoura et al. [2].

In the sections that follow, the control strategies discussed above, and variants thereof, are contrasted in WAMIT with the aim

of identifying a practical method that produces an accurate version of the desired wave system.

3. Numerical modelling of tank

3.1. Modelling in WAMIT

In the above section, theoretical expressions were presented for the paddle motions, and associated hydrodynamic torques, when a circular tank is generating planar waves. For modelling the behaviour of the tank under various force-control schemes however, one requires the wave elevations and hydrodynamic torque for *any* set of paddle amplitudes (and phases), which would be difficult to obtain analytically. The effects on the wave field of a body within the tank would also be difficult to express. Thus, to simulate wave generation and absorption in the tank, the approach of Newman [6], using numerical software WAMIT [21], is followed here and adapted to the parameters of FloWave TT. WAMIT is a frequency domain radiation/diffraction panel code based on potential flow theory, whose use in a range of hydrodynamic problems has been documented in literature (see, for example, [22–24]).

As in Newman [6], the linear version of WAMIT is applied here, in which the fluid velocity potential and hydrodynamic pressures are derived based on geometries corresponding to the rest state (the oscillation amplitudes of the body and the fluid are thus taken to be small). The higher-order method of solution is used, whereby the unknown velocity potential on the boundary surface is represented by continuous B-splines. The geometry of the submerged surface of the tank is defined analytically (assuming perfect cylindrical shape), with separate "patches" representing each of the wave-making paddles and the curved wall under the paddles (WAMIT subdivides "patches" further into "panels", which can be reduced in size by the user until a converged solution is attained).

The tank's $N = 168$ wave-maker segments are bottom hinged, flap-type devices with an approximate width of $b = 0.5$ m, and hinge depth $H = 1.5$ m. In the WAMIT model, they are represented by vertical patches that are side-by-side, with no gaps in-between. The motion of each paddle is described by a generalised mode, which specifies the normal velocity on the paddle face as a function of vertical position.

In addition to defining the tank geometry and modes of motions, the wave frequencies (or periods) and field points of interest are specified. For the analyses here, 41 wave periods in the range of $\tau = 1, \ldots, 3$ s are used, representing the planned operating range of FloWave. A total of 3360 points are considered on the free surface, covering a "test zone" in the middle of the tank with a diameter of 15 m, corresponding to the intended test area in the real tank.

With the problem fully defined, WAMIT is instructed to compute the free surface elevations resulting from a single mode (i.e. the motion of a single paddle) and the added mass matrix for all modes (giving the hydrodynamic coupling between the paddles). Note that the values for added damping are, in theory, zero, as a single oscillating paddle in a closed tank (with reflective walls) can only produce standing waves in the steady state. Thus, there is no energy transferred away from the paddle, and the hydrodynamic pressures along the wave-maker are in phase with the motion (displacement) of the paddle (see Newman [6] for a more formal explanation of why there is no damping).

Thanks to the axial symmetry of the tank, the wave field produced by any given paddle may be obtained by rotating the wave field obtained for the reference mode, and scaling it according to the paddle amplitude. The contributions of the individual paddles may then be superimposed to get the total wave elevation over the test zone.

3.2. Post-processing

Post-processing is used here to determine the displacement amplitudes of the individual paddles, as governed by the wave-maker control scheme in action, enabling the wave elevations to be computed. For a general force-control scheme, the feedback loops around the paddles are as depicted in Fig. 4 (and specified in Eq. (13)), whereby each paddle receives separate command torque T_o and is also subject to an absorption mechanism (or filter Z_f).

3.2.1. Tank without model in water

Considering the case when there is no model in the tank, the wave exciting torque T_w experienced by a paddle is then solely due to waves generated by other paddles. Thus, re-writing Eq. (13), the motion of a given paddle j is expressed in the frequency domain as

$$i\omega\theta(\omega)(Z_d(\omega)+Z_f(\omega)) - \omega^2 \sum_{k=1, j\neq k}^{N} r_{jk}\theta_k(\omega) = T_{o,j}(\omega), \tag{35}$$

where $r_{jk} = r_{kj}$ denotes the added inertia on paddle j as a result of the motion of paddle k, and the paddle rotations $\theta_k(\omega)$, $k = 1, \ldots, N$, are defined as positive when turning into the water, as indicated in Fig. 3.

For simplicity, it is assumed that Z_f is equal for all paddles and is of the form given by Eq. (16), in which case Eq. (35) becomes

$$-\omega^2 \sum_{k=1}^{N} r_{jk}\theta_k(\omega) + (-\omega^2(m_f + r) + i\omega d_f + c + c')\theta_j(\omega) = T_{o,j}(\omega), \tag{36}$$

or in terms of the linear displacement $X_{o,k}$ of the paddles at the still water level

$$-\omega^2 \sum_{k=1}^{N} A_{jk}X_{o,k}(\omega) + \frac{(-\omega^2(m_f + r) + i\omega d_f + c + c')X_{j,k}(\omega)}{H^2} = \frac{T_{o,j}(\omega)}{H}, \tag{37}$$

where $A_{jk} = r_{jk}/H^2$ are the equivalent added mass coefficients, as far as linear motion is concerned.

Eq. (37) can be written in matrix form as:

$$(p\mathbf{I} - \omega^2\mathbf{A})\mathbf{x} = \frac{1}{H}\mathbf{T_o}, \tag{38}$$

where $\mathbf{I}$ is the identity matrix, $\mathbf{A}$ is the matrix of added mass coefficients, $\mathbf{x}$ and $\mathbf{T_o}$ are the vectors of paddle displacements and command torques, and p is a parameter given by

$$p = \frac{-\omega^2(m_f + r) + i\omega d_f + c_f + c'}{H^2}. \tag{39}$$

One therefore has a matrix equation that can be solved for the paddle motions $X_{o,k}$ for a given absorption mechanism, command torques and added mass coefficients A_{jk} (the latter being provided by the WAMIT model):

$$\mathbf{x} = \frac{1}{H}(p\mathbf{I} - \omega^2\mathbf{A})^{-1}\mathbf{T_o}. \tag{40}$$

3.3. Tank with floating body

Assume that a freely floating sphere of radius R_b is now introduced into the tank, as in Newman [6]. The added mass matrix $\mathbf{A}$ changes to $\mathbf{A}'$ as a result and additional modes, corresponding to the oscillation of the sphere, need to be considered. In the basic scenario of generating waves in the direction of the x-axis (which is generalisable to all directions, thanks to the symmetry of the tank and floating body), there are two extra modes to account for: the

surging X_b and heaving Z_b motions of the body. Denoting the added mass of these modes by A_{xx}, A_{zz}, and cross-coupling between the sphere and the wave-makers by A_{xk}, A_{zk}, $k = 1, \ldots, N$, the equations of motion for the modified system can be expressed as

$$\left(p \begin{bmatrix} \mathbf{I} & 0 & 0 \\ 0 & -\omega^2 m_b & 0 \\ 0 & 0 & C_z - \omega^2 m_b \end{bmatrix} - \omega^2 \begin{bmatrix} \mathbf{A}' & \mathbf{A_x^T} & \mathbf{A_z^T} \\ \mathbf{A_x} & A_{xx} & 0 \\ \mathbf{A_z} & 0 & A_{zz} \end{bmatrix} \right) \begin{bmatrix} \mathbf{x} \\ X_b \\ Z_b \end{bmatrix} = \frac{1}{H} \begin{bmatrix} \mathbf{T_o} \\ 0 \\ 0 \end{bmatrix}, \tag{41}$$

where $C_z = \pi R_b{}^2$ is hydrostatic restoring coefficient for the heaving sphere, m_b is the mass of the sphere and $\mathbf{A_x} = [A_{x1} \ldots A_{xN}]$, $\mathbf{A_z} = [A_{z1} \ldots A_{zN}]$.

The control scheme proposed by Newman [6] will now be considered, in which the wave-maker is "calibrated" (command torques $T_{o,j}$ set) with no model in the tank, and the absorption mechanism is programmed to react only to the *difference* between the anticipated and sensed hydrodynamic torques on the paddles. Newman [6] does not specify explicitly how the scheme would be implemented in practice, but a realistic approach would be for the absorption filter Z_f in Fig. 4 to be fed the difference between the calibrated and measured paddle velocities. In this case, taking $\tilde{\mathbf{x}}$ as the vector of calibrated paddle displacements, and $\mathbf{x} = \tilde{\mathbf{x}} + \boldsymbol{\delta}\mathbf{x}$ as the paddle motions with the sphere present, one may write

$$\left(p \begin{bmatrix} \mathbf{I} & 0 & 0 \\ 0 & -\omega^2 m_b & 0 \\ 0 & 0 & C_z - \omega^2 m_b \end{bmatrix} - \omega^2 \begin{bmatrix} \mathbf{A}' & \mathbf{A_x^T} & \mathbf{A_z^T} \\ \mathbf{A_x} & A_{xx} & 0 \\ \mathbf{A_z} & 0 & A_{zz} \end{bmatrix} \right) \begin{bmatrix} \mathbf{x} \\ X_b \\ Z_b \end{bmatrix} = \frac{1}{H} \begin{bmatrix} \mathbf{T_o} \\ 0 \\ 0 \end{bmatrix} + Z_f \begin{bmatrix} \tilde{\mathbf{x}} \\ 0 \\ 0 \end{bmatrix}. \tag{42}$$

For the calibrated tank (without the floating body) there is no action from the absorption mechanism so that, from Eq. (38), the command torques are:

$$\frac{1}{H}\mathbf{T_o} = \left(\frac{(-\omega^2 r + c')\mathbf{I}}{H^2} - \omega^2 A \right) \tilde{\mathbf{x}}. \tag{43}$$

Substituting this into Eq. (42), the right hand side becomes

$$\left(\frac{(-\omega^2 r + c')\mathbf{I}}{H^2} - \omega^2 \mathbf{A} \right) \begin{bmatrix} \tilde{\mathbf{x}} \\ 0 \\ 0 \end{bmatrix} + \frac{(-\omega^2 m_f + i\omega d_f + c')}{H^2} \begin{bmatrix} \tilde{\mathbf{x}} \\ 0 \\ 0 \end{bmatrix} = (p\mathbf{I} - \omega^2 \mathbf{A}) \begin{bmatrix} \tilde{\mathbf{x}} \\ 0 \\ 0 \end{bmatrix},$$

which enables Eq. (42) to be re-written as

$$\left(p \begin{bmatrix} \mathbf{I} & 0 & 0 \\ 0 & -\omega^2 m_b & 0 \\ 0 & 0 & C_z - \omega^2 m_b \end{bmatrix} - \omega^2 \begin{bmatrix} \mathbf{A}' & \mathbf{A_x^T} & \mathbf{A_z^T} \\ \mathbf{A_x} & \mathbf{A}_{xx} & 0 \\ \mathbf{A_z} & 0 & A_{zz} \end{bmatrix} \right) \begin{bmatrix} \boldsymbol{\delta}\mathbf{x} \\ X_b \\ Z_b \end{bmatrix} = -\omega^2 (\mathbf{A} - \mathbf{A}') \begin{bmatrix} \tilde{\mathbf{x}} \\ 0 \\ 0 \end{bmatrix}, \tag{44}$$

allowing the new paddle motions $\mathbf{x} = \tilde{\mathbf{x}} + \boldsymbol{\delta}\mathbf{x}$ (and the sphere surge and heave motions) to be calculated. This equation is similar to Eq. (37) in Newman [6], but that equation assumes that the sphere is fixed ($X_b = Z_b = 0$).

4. Simulation results

The results of WAMIT simulations are presented below, contrasting the performance of the following force-control schemes:

1) The control scheme in which the paddles are oscillated with prescribed amplitudes (as per Eq. (23)) so as to conform to the desired progressive wave field. The required command torques $\mathbf{T_o}$ are computed using Eq. (38), with $\mathbf{A}$ being the added mass matrix given by WAMIT for the tank. Note that this scheme is highly idealised, as it assumes that the signals prescribed to the "absorbing paddles" cancel out exactly the waves originating from the "generating paddles".
2) The more sophisticated (but untested) scheme of Newman [6] whereby paddles are oscillated as in method 1 (with the same command torques $\mathbf{T_o}$) but where every paddle is equipped with an absorption mechanism that responds to deviations from the expected hydrodynamic torques on the paddles
3) The control scheme of Minoura et al. [2], as used in the AMOEBA tank, in which each paddles as an identically programmed absorption filter Z_f (responding to the absolute motion of the paddle), and the command torques $\mathbf{T_o}$ for generating a planar wave are as given by Eq. (34) (with the transfer function $I(\omega)$ being determined numerically using WAMIT).

To compare the above control strategies, the generation of straight, plane regular waves of different frequencies will be considered, remembering that due to the axisymmetry of the tank, complex multi-directional wave fields, simulating real sea states, can be created by superimposing these waves. In particular, the effectiveness of the schemes in producing waves with uniform, Pierson–Moskowitz (PM) [25], and JONSWAP [26] spectra is investigated. The spectral density of JONSWAP is of the form

$$S(\omega) = \frac{1}{\omega^5} \exp\left\{ -\frac{5}{4} \left(\frac{\omega_p}{\omega} \right)^4 \right\} \gamma^r, \quad r = \exp\left\{ -\frac{(\omega - \omega_p)^2}{2\sigma^2 \omega_p^2} \right\}, \tag{45}$$

where ω_p is the peak frequency and the parameters γ, σ are given by

$$\gamma = 3.3, \quad \sigma = \begin{cases} 0.07 & \text{for } \omega \le \omega_p, \\ 0.09 & \text{for } \omega > \omega_p. \end{cases} \tag{46}$$

A PM spectrum is obtained by removing the peak enhancement factor γ^r from the above equation.

Here the peak frequency is taken to be $\omega_p = \pi$ rad/s, corresponding to the frequency that FloWave is to be optimised for. Recalling that the absorption filter Z_f can only provide optimum absorption at a single chosen frequency, two sets of filter coefficients will be considered in methods 2 and 3:

approach a) Coefficients tuned to the peak frequency ω_p (according to 2D wave-maker theory)
approach b) Coefficients obtained by least squares fitting Z_f to the optimal impedance (as per 2D theory) over the design frequency range of $\omega = 2\pi/3$ to 2π rad/s (wave periods of 1 s to 3 s).

For the paddle geometry of FloWave, the above approaches yield the following coefficients (assuming a water density of $\rho = 1000\,\mathrm{kg\,m^{-3}}$):

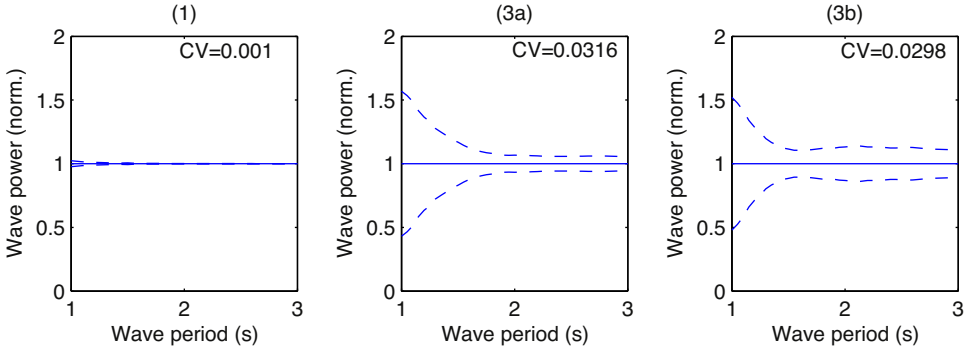

Fig. 8. Generation of uniform spectrum using three methods: (1) paddles are moved with pre-set drive signals, no absorption mechanism (3a) absorption mechanism tuned to 2 s waves (3b) absorption mechanism optimised for 1–3 s range.

approach a) $m_f + r = -r_\Phi(\omega_p) = -38.6\,\mathrm{kg\,m^2}$,
$d_f = d_\Phi(\omega_p) = 1440\,\mathrm{kg\,m^2\,s^{-1}}$, $c_f + c' = 0$.
approach b) $m_f + r = -23.2\,\mathrm{kg\,m^2}$, $d_f = 1271\,\mathrm{kg\,m^2\,s^{-1}}$,
$c_f + c' = 269\,\mathrm{kg\,m^2\,s^{-2}}$.

4.1. Tank without model in water

With no objects in the tank, the wave field over the "test zone" should be as uniform as possible. Thus one way of assessing the quality of the wave field is by evaluating the spatial variability of the wave amplitude, or in the case of a multi-frequency wave, the variability of the wave spectrum in the tank (another way of quantifying the deviation of the generated waves from the desired long-crested waveforms would be in terms of the wave *direction*, but this will not be considered here).

Considering a wave field composed of a finite number of frequencies, one may express the (discretised) wave spectrum by $S_n(\omega_k)$, where the index n refers to the field points, and ω_k denotes the different frequencies. Note that at any given field point, $S_n(\omega_k)$ is proportional to the *square* of the wave amplitude at ω_k. With reference to this spectrum, the following measure of wave field quality is adopted

$$CV = \frac{\sqrt{\sum_k sd^2(S_n(\omega_k))}}{\sum_k \overline{S_n}(\omega_k)}. \tag{47}$$

In other words, the variance (squared standard deviation) across the field points of the spectral components is summed and the square root of the result is taken. A normalisation factor, corresponding to the sum of the components of the mean wave spectrum, is then applied. The resulting coefficient *CV* gives the "relative standard deviation" of the sum of the spectral components, and the lower its value, the more uniform the wave field is within the specified domain.

Fig. 8 shows the wave spectra across the test zone, as obtained using methods 1, 3a and 3b, when a uniform wave spectrum is generated (for an "empty" tank, methods 1 and 2 give identical results, as there is no action from the absorption mechanism in the latter). In each case, three lines are given, showing the mean wave spectrum (full line), together with ±1 standard deviation bands (dashed lines), and the *CV* value is stated. At each frequency, an adjustment factor has been applied to the paddle signals to ensure that the mean spectrum matches the target spectrum exactly.

One can see from the graphs that method 1, in which all the paddles are sent pre-set drive signals and there is no absorption mechanism, performs best. The three lines in the corresponding plot are practically coincident, indicating that the target spectrum is reproduced uniformly throughout the specified "test zone" in the tank. However, as discussed above, this method is too "idealistic" in practice. Amongst the two more "realistic" schemes, method 3b (with absorption optimised for the whole frequency range) gives marginally better wave uniformity overall than method 3b (in which absorption is tuned to the middle frequency). That being said, both methods fail to reproduce the short wave period (high frequency) end of the target wave spectrum in a consistent way, the corresponding standard deviation being over 0.5. This is due to a rapid variation in radiation impedance as one approaches this end of the spectrum, resulting in a significant mismatch with respect the absorption filter impedance, which in turn causes wave reflections and standing waves in the tank.

It is interesting to observe what happens when the absorption is instead tuned for the short wave period end (1 s waves) of the spectrum. Fig. 9 shows the corresponding results. In this case, there is high spatial variability throughout the spectrum, apart from at the shortest of wave periods. Carrying out further simulations reveals that there is not a single set of absorption filter coefficients that provides effective absorption over the entire wave spectrum (representing the designed operating range of the tank). In practice, the absorption mechanism will need to be adjusted according to the spectrum to be generated.

Figs. 10 and 11 present the results for the generation of PM and JONSWAP spectra, respectively. Method 1, relying on the anticipation and perfect cancellation of incident waves by the "downstream" paddles, again results in an essentially uniform wave field (in terms of amplitude at least). The small deviations in the wave field are due to wave-maker segmentation effects (numerical errors in the calculations may also be partly responsible). With absorption carried out by a dynamic absorption mechanism, tuning the mechanism to the peak frequency (Method 3a) gives a more consistent wave spectrum as compared with optimising over the entire frequency range (Method 3b). Notice that the *CV* values are considerably lower for Method 3a, by as much as 75% in the

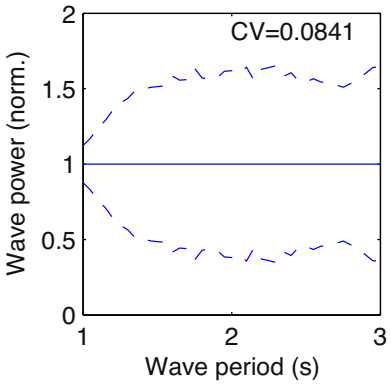

Fig. 9. Generation of uniform spectrum when absorption is tuned to 1 s waves.

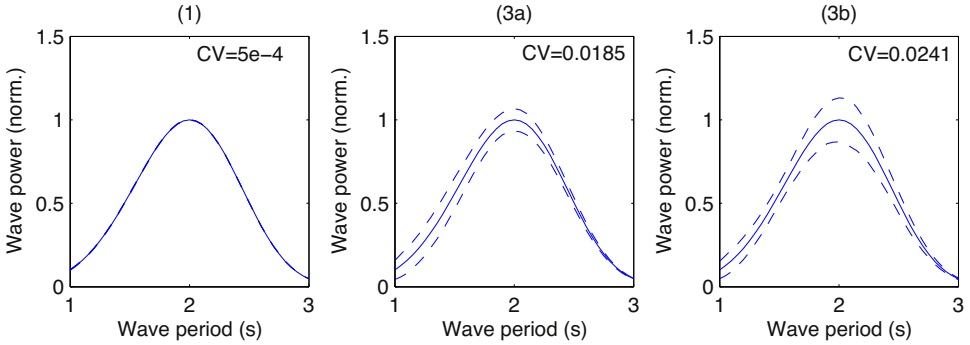

Fig. 10. Generation of PM spectrum using three methods: (1) paddles are moved with pre-set drive signals, no absorption mechanism (3a) absorption mechanism tuned to 2 s waves (3b) absorption mechanism optimised for 1–3 s range.

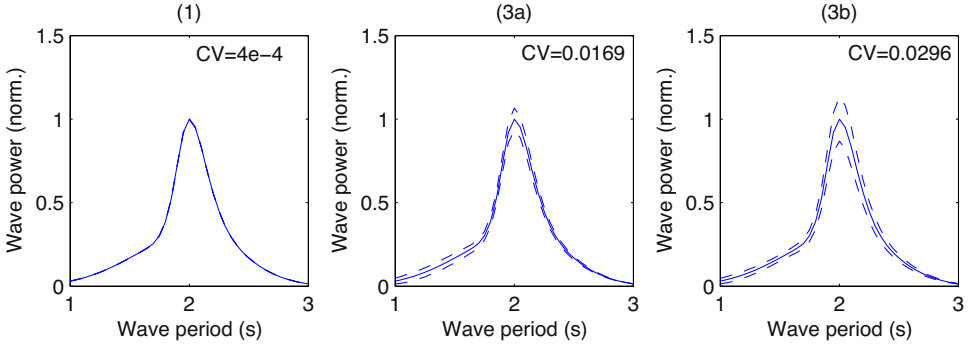

Fig. 11. Generation of JONSWAP spectrum using three methods: (1) paddles are moved with pre-set drive signals, no absorption mechanism (3a) absorption mechanism tuned to 2 s waves (3b) absorption mechanism optimised for 1–3 s range.

case of JONSWAP. One can also observe that the poor performance of the absorption mechanisms for short wave periods (as noted when generating uniform spectra) is less apparent in these figures, thanks to lower spectral content at short wave periods. Both Method 3a and Method 3b manage to reproduce the "shape" of the target distribution, whether the target wave spectra is PM or JONSWAP.

Matsumoto et al. [27] suggest applying non-linear, least-squares optimisation to the paddle signals as a means of improving the uniformity of monochromatic, oblique waves in a rectangular wavetank. In the proposed method, the displacement amplitudes of the paddles (which are taken to be position-controlled) are adjusted iteratively so as to minimise the error in wave height (desired versus measured) over a specified area in the tank. Numerical and experimental results are given, indicating significant improvement in the uniformity of not just wave height, but also of wave propagating direction.

Preliminary results of simulations carried out here suggest that this optimisation method may be extended to the circular tank geometry (and force-feedback paddles) of FloWave. With the tank initially configured to generate waves as per Method 3a, optimising the torque command signals of the upstream paddles at a given wave frequency (within the operating range) enables an at least 20% reduction in the standard deviation of wave height over the test zone. However, care must be taken in the choice of sample points over which wave height is optimised. If the points are "few and far between", then the optimised wave field will show considerable height variations in between points, whilst a large number of sample points make the optimisation task computationally demanding. In any case, wave uniformity outside the region of interest can deteriorate drastically. Until a suitable strategy is identified for dealing with these issues, the implementation of the optimisation technique for FloWave may prove impractical.

4.1.1. Paddle malfunction

Additional simulations were conducted looking at the effect of a single paddle malfunctioning on wave field uniformity. Three different types of faults were considered, in the context of the generation of uni-directional JONSWAP spectrum using Method 3a:

i. "Stuck" paddle (no paddle motion)
ii. Faulty tachogenerator (zero velocity measurement)
iii. Uncontrolled paddle (no control torque)

(Another possible fault would be the load cell giving zero reading, but that would likely lead to excessively large control torques being applied on the paddle, leading to unstable behaviour).

In cases ii and iii, the generated wave amplitudes were taken to be sufficiently small for the stroke of the faulty paddle to remain within the "linear operating range". The following paddle parameters were assumed (representing ballpark figures):

1. Inertia of $r = 22.5\,\mathrm{kg\,m^2}$
2. Effective mechanical stiffness $c' = 450\,\mathrm{kg\,m^2\,s^{-2}}$

Fig. 12 plots the change in *CV* value resulting from the different faults, as compared with the faultless case, against the position – or angle φ_j – of the affected paddle (note that paddles in the range $90^\circ < \varphi_j < 180^\circ$ act as generators, whilst those in $0^\circ < \varphi_j < 90^\circ$ are absorbers in this example). It is observed that the increase in the variability of the wave field, as quantified by *CV*, depends greatly on the type of fault, ranging from a modest, maximum increase of 20% in the case of a stuck paddle, to a more substantial, potentially two-fold increase in *CV* for a faulty tachogenerator or uncontrolled paddle. For all three types of faults, the exact change in *CV* is heavily influenced by the position of the paddle relative to the direction of the generated wave.

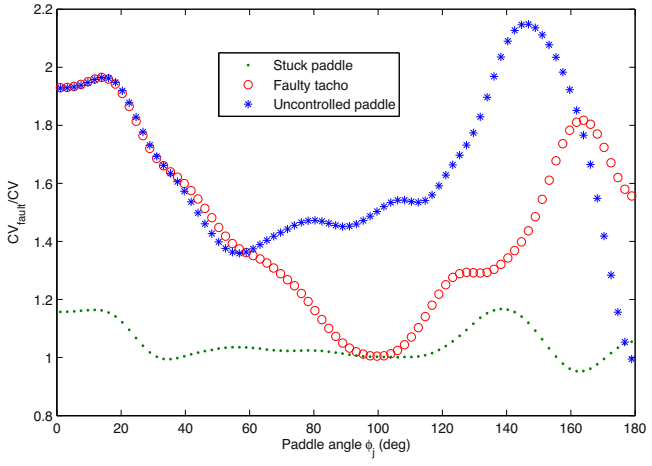

Fig. 12. The effect of different paddle faults on wave field variability.

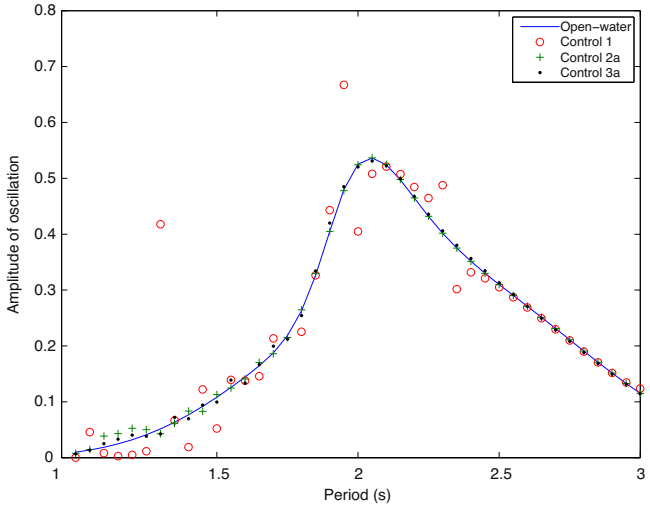

Fig. 13. Surge motion of sphere for JONSWAP wave in the open-water case and for the control schemes: (1) paddles are moved with pre-set drive signals, no absorption mechanism (2a) absorption mechanism that reacts to deviation in hydrodynamic torques on paddles (3a) basic absorption mechanism.

It is interesting to note the similarity in the results for the faulty tachogenerator and uncontrolled paddle, when the affected paddle is amongst the "absorbers" located at $\varphi_j < 45^\circ$. For these paddles, there are no specified command torques, the control signal being purely composed by the absorption filter, and derived from velocity feedback. Hence, in the absence of a velocity signal, no control torque is applied on the paddle.

4.2. Tank with floating object

The scenario is now considered (as in Newman [6]) whereby a floating sphere, of radius $R_b = 1$ m and half the density of the water, is placed in the middle of the tank. As a result, the incident waves generated by the wave-maker are scattered, and there are radiated waves arising from the motion induced in the object. These radiated and scattered waves propagate towards the perimeter and must be absorbed by the wave-maker rather than reflected back (so as to ensure that only the prescribed waves are incident on the sphere).

Due to the additional waves in the tank, judging the effectiveness of the wave-maker control by uniformity of the overall wave field is not practical. Instead, it is more useful to assess the hydrodynamic forces on the sphere, comparing these to the "open-water" case (which can also be simulated in WAMIT), when there are no tank boundaries and planar waves are incident on the sphere. An equivalent approach to considering the resultant forces is to evaluate the motions of the body, and it is the latter approach that is taken here. Bearing in mind the symmetry of the tank, there are two motions to account for, surge and heave, when generating waves in the direction of the x-axis.

Fig. 13 contrasts the surge motions, as a function of wave period, resulting from the paddle control methods 1, 2a and 3a, to those calculated for the open-water case when a JONSWAP spectrum is generated. The results for the corresponding heave motions are plotted in Fig. 14. On both graphs, the displacement amplitudes are normalised by the prescribed wave amplitude at the peak frequency ($\omega_p = \pi$ rad/s, corresponding to a 2 s wave period).

It is apparent from Figs. 13 and 14 that method 1, in which the paddle drive signals are pre-set and there is no absorption mechanism, is inadequate for reproducing a JONSWAP sea when a body is present in the tank. Conversely, the results of methods 2a and 3a are in good agreement with those for the desired sea.

To quantify the errors (or deviations) in the body motions with respect to the open-water case, the absolute value of the error in displacement amplitude is summed up over all the frequencies to obtain a measure of the overall error for each mode:

$$Err = \frac{\sum_k |\xi(\omega_k) - \xi_o(\omega_k)|}{\sum_k |\xi_o(\omega_k)|}, \tag{48}$$

where $\xi(\omega_k)$ is the amplitude of the body displacement (in heave or surge) at frequency ω_k for the given control scheme, and $\xi_o(\omega_k)$ is the corresponding open-water amplitude.

For method 1, the heave and surge motions of the body differ considerably from those in the open-water case (the total errors are $Err_1 = 0.6518$ and 0.5954, respectively) and display resonant behaviour at several wave periods (note that the computed surge amplitude at a period of 1.75 s, $\xi = 5.077$, and the heave amplitude at 1.95 s, $\xi = 5.126$, are outside the range plotted). Whilst WAMIT ignores viscous effects, which in practice temper resonant behaviour, real-life results would also likely to show significant errors in the body motions for this naïve control scheme. On the other hand, the curves for control Schemes 2a and 3a both follow

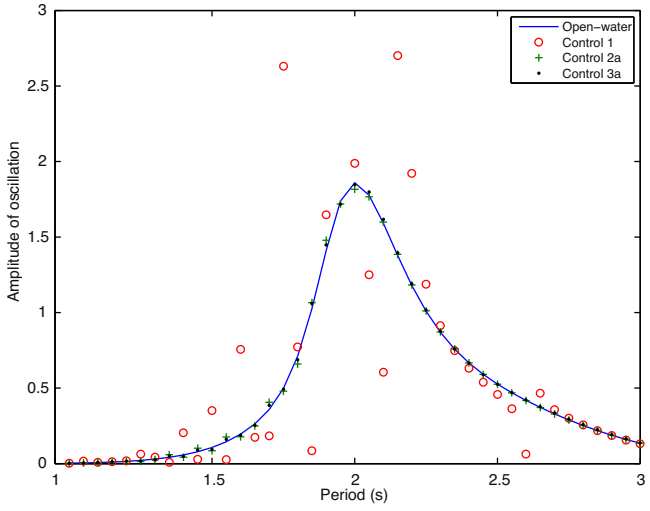

Fig. 14. Heave motion of sphere for JONSWAP wave in the open-water case and for the control schemes: (1) paddles are moved with pre-set drive signals, no absorption mechanism (2a) absorption mechanism that reacts to deviation in hydrodynamic torques on paddles (3a) basic absorption mechanism.

the open-water results closely, with most of the discrepancies being in the short period range. For these control schemes the surge and heave errors in the body motions are $Err_{2a} = 0.0132$, 0.0220 and $Err_{3a} = 0.0213$, 0.0171.

The above simulation results suggest that, as far as the body forces are concerned, Scheme 3a is able to reproduce JONSWAP seas to a similar level of accuracy as the more complex method 2a, for a spherical body placed in the middle of the tank.

5. Non-linear waves

This study considers the control of the wave tank only from the perspective of linear waves. There is, in effect, an inherent assumption that the waves generated in the tank are of low amplitude. However much of the interest when undertaking physical tests in fact lies in nonlinear fluid/structure interactions, which can be difficult to model reliably using analytical or numerical approaches. Thus it becomes important for the tank to be able to successfully reproduce not only low amplitude waves, but also sea states with non-linear, high steepness (or extreme) waves, in an accurate way (for which successful linear generation is only a prerequisite).

To that end, one must ensure that unnatural "free waves" – harmonics of the main wave travelling at a slower phase velocity – are minimised (in the case of a multi-chromatic waves, free waves will also exist for sub- and super-harmonic interactions). These are artefacts[1] of laboratory wave-making that result from a mismatch between the orbital velocity corresponding to the bound harmonics – travelling along with the main wave – and the velocity profile of the wave-maker at the boundary of the tank.

Suppressing spurious waves requires appropriate wave-maker design, such that the kinematics of the wave board conform to the waves to be generated in the tank. The control strategy in use, and whether some form of higher-order compensation is applied to the drive signal of the paddles, can also play an important role in determining the amount of free waves produced in the tank.

For the round tank studied here, to assess numerically the effectiveness of different control schemes in producing non-linear waves, one would need to depart from the first-order BEM model, and instead use a higher-order approach. Remaining within the realm of potential flow theory, the Higher-Order Spectral (HOS) method of Ducrozet et al. [11] would be a viable option for such an analysis. Unlike many numerical wave tanks, this model accounts for the features of a real basin, so that the propagation domain is bounded, and waves are generated by a wave-maker. Fully non-linear free surface conditions are assumed, and the wave-maker is modelled to third order. Note however that to apply HOS to FloWave would require modifications to the basic methodology, which currently assumes position-controlled paddles, driven by first-order command signals, rather than the force-controlled absorbing wave boards of FloWave.

For a set of paddles in a straight line, producing an oblique wave, the second-order, second-harmonic free wave component may be readily estimated using the analytical theory of Schaffer et al. [28]. This theory suggests that for a typical flap-type wave-maker, operated in first-order position-control, the free wave can be as large as the bound second-harmonic for some wavelengths. The free wave will also be oblique, but propagating in a different (less oblique) direction to the main wave.

Considering now a round tank, the generated free wave will in this case be affected by not only the curvature of the paddle faces, but also by the varying stroke size around the rim. Thus complex second-order wave elevation patterns may emerge. The use of force rather than position-control on the paddles will likely lead to a reduction in the generated free waves (as the wave-maker "senses" and tends to compensate for some of the free waves [4]). Furthermore, with force-control, the spurious waves will be partially absorbed as they reach the boundaries of the tank (albeit not necessarily very effectively, as the absorption capability of the paddles is reduced at higher frequencies). In any case, the results presented in the preceding section represent an upper-bound on the level of performance that may be expected from the tank in reproducing sea spectra.

6. Conclusions

The main aim of this study has been to identify suitable control strategies for reproducing sea spectra in a force-controlled circular wave tank, with a particular emphasis on the University of Edinburgh's FloWave TT basin.

As part of the study, a detailed review has been carried out of the hydrodynamic theory relating to control of a circular wave tank. In the case of a tank free of any objects, the theoretical torques to be applied on the paddles to generate planar, regular waves are found to be similar to those calculated numerically using WAMIT. When a floating object is present in the tank (as in normal operation), scattered and radiated waves arise, which must be absorbed at the perimeter of the tank. Thus some form of absorption mechanism must be incorporated in the paddle controls.

Two different control schemes offering absorption have been evaluated here. The scheme of Minoura et al. [2], as implemented in the AMOEBA tank, prescribes wave-generating forces on the "upstream paddles", and each paddle has an identically tuned dynamic absorption mechanism. The more complex method of Newman [6] (untested in practice), imposes pre-set command torques on all the paddles, and has an absorption mechanism that reacts to deviations in the sensed hydrodynamic forces on the paddles as compared with the "empty" tank.

In numerical simulations, both methods are found to reproduce multi-chromatic (JONSWAP) seas effectively, in so far as the behaviour of a freely floating object in the tank is concerned. For both control schemes, the motions induced in the object are very close to the results for the "open-water" case (the overall error in the displacement amplitudes being around 2% with both schemes).

Important observations may be made relating to the uniformity of wave fields across the tank. With specific relevance to experimentation in the FloWave tank, it is noted that when generating multi-chromatic seas, the scheme of Minoura et al. [2] produces a more spatially-uniform wave field with the absorption tuned to the peak frequency rather than optimised for the entire frequency range. Furthermore, tuning absorption to the middle of the design range (0.5 Hz waves), results in inadequate absorption (and so non-uniform waves) at the high frequency end (1 Hz waves), and vice versa. There is not a single absorption setting that works effectively across the entire design frequency range, which may necessitate the use of wave absorbing beaches in some experiments involving "wide" spectra.

One possibility would be to use floating, porous blocks [29], which can be made to be highly effective at absorbing higher frequencies in a wave basin, whilst transmitting lower frequencies. In FloWave, these would be positioned in front of the arc of paddles not taking part in the wave generation, but only functioning as absorbers in the given test. Thus, provided the generated wave spectrum has a suitably narrow spread, high frequency components would be intercepted and removed by porous blocks on arrival at the opposite side of the tank. Lower frequencies (and any currents) would pass through unimpeded, to be absorbed by the paddles behind the porous blocks.

[1] Another higher-order artefact of wave-making in an enclosed domain is the return current that is established due to mass transport in the direction of the waves (as described by the Stokes drift).

In a tank with such a large number of wave paddles it becomes useful to assess the impact of a faulty paddle. The use of WAMIT also allows for typical paddle faults to be simulated in a straightforward way. It is found that even the malfunction of a single paddle can have a marked impact on the uniformity of the wave field in the tank. For example, with a JONSWAP sea being the target, the standard deviation of the generated spectrum can double if a paddle's velocity sensor fails. Thus, all paddles should function well to ensure accurate reproduction of wave fields.

All the results presented here assume linear waves in the tank. Whilst this helps considerably in assessing different control schemes, an effective wave basin must be able to produce nonlinear waves as well. The next stage in this work should therefore be to incorporate higher-order effects in the simulation of control strategies. There are also plans for simulation results to be validated experimentally. Furthermore, the effects of currents on the generated wave field, and indeed how these may be compensated for in the wave-maker control system, are to be investigated. The possibility of adjusting control parameters "on the fly", based on measurements of directional wave spectra in the tank, is also of interest.

Acknowledgments

The authors would like to express their gratitude to David Forehand, Gregory Payne, and Johannes Spinneken for their invaluable advice on the modelling of wave tanks. The authors are also indebted to John N. Newman, who kindly shared WAMIT code corresponding to his paper on the subject. They would also like to acknowledge the support of EPSRC in funding this work (grant number EP/H012745/1).

References

[1] Maeda K, Hosotani N, Tamura K, Ando H. Wave making properties of circular basin. In: International symposium on underwater technology: IEEE. 2004. p. 349–54.
[2] Minoura M, Naito S, Muto T, Okuyama E. Generation of arbitrary wave field in arbitrarily configured wave basin composed of element-absorbing wavemakers. Int J Offshore Polar Eng 2011;21(4):272–9.
[3] Davey T, Bryden I, Ingram D, Robinson A, Sinfield J, Wallace A. The All-Waters Test Facility – a new resource for the marine energy sector. In: ICE breakwaters '13. 2013.
[4] Spinneken J, Swan C. The operation of a 3D wave basin in force control. Ocean Eng 2012;55:88–100.
[5] Salter S. Absorbing wave-makers and wide tanks. In: Directional wave spectra applications: ASCE. 1981. p. 185–202.
[6] Newman JN. Analysis of wave generators and absorbers in basins. Appl Ocean Res 2010;32:71–82.
[7] Gyongy I, Richon J-B, Bruce T, Bryden I. Validation of a hydrodynamic model for a curved, multi-paddle wave tank. Appl Ocean Res 2014;44: 39–52.
[8] Dalrymple R, Greenberg M. Directional wave makers. In: Physical modelling in coastal engineering. Rotterdam: A.A. Balkema; 1985. p. 67–81.
[9] Takayama T. Theoretical properties of oblique waves generated by serpent-type wavemakers. Rep Port Harb Res Inst 1982;21:3–48.
[10] Dalrymple RA. Directional wavemaker theory with sidewall reflection. J Hydraul Res 1989;27:23–34.
[11] Ducrozet G, Bonnefoy F, Le Touze D, Ferrant P. A modified High-Order Spectral method for wavemaker modeling in a numerical wave tank. Eur J Mech B-Fluid 2012;34:19–34.
[12] Spinneken J, Swan C. Second-order wave maker theory using force-feedback control, Part I: A new theory for regular wave generation. Ocean Eng 2009;36:539–48.
[13] Naito S. Wave generation and absorption in wave basins: theory and application. Int J Offshore Polar Eng 2006;16(2):81–9.
[14] Spinneken J, Swan C. Theoretical transfer function for force-controlled wave machines. Int J Offshore Polar Eng 2011;21:169–77.
[15] Falnes J. Ocean waves and oscillating systems. Cambridge, UK: Cambridge University Press; 2002.
[16] Maguire AE [PhD thesis] Hydrodynamics, control and numerical modelling of absorbing wavemakers. Edinburgh, UK: Univ. Edinburgh; 2011.
[17] Spinneken J, Swan C. Wave generation and absorption using force-controlled wave machines. In: 19th international offshore and polar engineering conference, vol. 3. 2009. p. 397–404.
[18] Chatry G, Clement AH, Gouraud T. Self-adaptive control of a piston wave absorber. In: 8th international offshore and polar engineering conference, vol. 1. 1998. p. 127–33.
[19] Mei CC, Zhou X. Wave-making by the rim of a circular basin. Appl Ocean Res 1991;13:37–42.
[20] Naito S, Minoura M, Okuyama E. Diffraction force in compact basin with absorbing wave maker. Int Offshore Polar Eng 2002;39:9–405.
[21] Lee C, Newman J. WAMIT® user manual, version 7.0 PC; 2012.
[22] Clauss GF, Birk L. Hydrodynamic shape optimization of large offshore structures. Appl Ocean Res 1996;18:157–71.
[23] Lee S, Kim M, Lee D, Kim J, Kim Y. The effects of LNG-tank sloshing on the global motions of LNG carriers. Ocean Eng 2007;34:10–20.
[24] Payne GS, Taylor JRM, Bruce T, Parkin P. Assessment of boundary-element method for modelling a free-floating sloped wave energy device. Part 1: Numerical modelling. Ocean Eng 2008;35:333–41.
[25] Pierson WJ, Moskowitz L. A proposed spectral form for fully developed wind seas based on the similarity theory of SA Kitaigorodskii. J Geophys Res 1964;69(24):5181–90.
[26] Hasselmann K, Barnett TP, Bouws E, Carlson H, Cartwright DE, Enke K, et al. Measurements of wind-wave growth and swell decay during the Joint North Sea Wave Project (JONSWAP); 1973.
[27] Matsumoto A, Hanzawa M. New optimization method for paddle motion of multi-directional wavemaker. In: 25th international conference on coastal engineering, Part I. 1996. p. 479–92.
[28] Schaffer HA, Steenberg CM. Second-order wavemaker theory for multidirectional waves. Ocean Eng 2003;30:1203–31.
[29] Robinson A. An effective frequency dependent filter for removing selected fluid surface waves from wave-fields and wave-trains; 2014 [submitted for publication].